Exploiting the Properties of Reciprocal Filter in Low-Complexity OFDM Radar Signal Processing Architectures

JAVIER TRUJILLO RODRIGUEZ, Student Member, IEEE
GIOVANNI PAOLO BLASONE, Member, IEEE
FABIOLA COLONE, Senior Member, IEEE
PIERFRANCESCO LOMBARDO, Senior Member, IEEE
Sapienza University of Rome, Rome, Italy

This article explores signal processing architectures for disturbance cancellation and range-Doppler map evaluation in orthogonal frequency division multiplexing (OFDM) radar. The signal processing chain of an OFDM radar typically encompasses a disturbance cancellation stage followed by the range-Doppler map evaluation, which can be in turn decomposed into a range compression stage performed at OFDM symbol level and a Doppler processing across symbols. In this article, we use a reciprocal filter (RF) to perform the range compression and we deepen the understanding of the RF properties with particular reference to their impact on the other processing stages of the signal processing scheme, above all disturbance cancellation. By exploiting this understanding, we show that it is possible to create synergies between different processing stages, even swapping their order, with the aim to improve the performance of the system while keeping limited its complexity. Thanks to this strategy, alternative versions of existing disturbance cancellation algorithms can be considered that would not be feasible in conventional architectures. Moreover, this article makes it possible to include within the same interpretative framework approaches that seem to be very distant from each other in terms of processing techniques thus allowing their throughout comparison both in terms of target detection performance and in terms of computational complexity. The performance of different solutions is investigated and compared against simulated and experimental data for the case of an OFDM radar that parasitically exploits DVB-T signals of opportunity.

Manuscript received 6 December 2022; revised 4 April 2023; accepted 24 May 2023. Date of publication 7 June 2023; date of current version 11 October 2023.

DOI. No. 10.1109/TAES.2023.3283489

Refereeing of this contribution was handled by K. S. Kulpa.

This work was supported by the European Union under the Italian National Recovery and Resilience Plan of NextGenerationEU, partnership on "Telecommunications of the Future" (PE00000001—program "RESTART," CUP B53C22004050001).

Authors' address: Javier Trujillo Rodriguez, Giovanni Paolo Balsone, Fabiola Colone, and Pierfrancesco Lombardo are with the Department of Information Engineering, Electronics and Telecommunications (DIET), Sapienza University of Rome, Rome 00184, Italy, E-mail: (javier.trujillorodriguez, giovannipaolo.blasone, fabiola.colone, pierfrancesco.lombardo@uniroma1.it). *(Corresponding author: Fabiola Colone.)*

I. INTRODUCTION

The popularity of orthogonal frequency division multiplexing (OFDM) radar [1] has increased rapidly in recent years being driven by two main aspects: the advancement in hardware capabilities and the growing demand for reciprocal filter (RF) spectral resources. With particular reference to the latter aspect, the use of OFDM signals as radar waveforms inherently facilitates the cohabitation between radar and communications systems using overlapping bandwidths. This has come to be a major investigation field in recent years and encompasses a number of paradigms depending on the level of integration between different functions, moving from coexistence of independent systems to codesign of fully integrated systems [2], [3], [4], [5]. Passive radar (PR) can be also included in this scenario as a pioneering form of coexistence where the sensing functionality is totally subject to the design of the communications system [6], [7]. Indeed, several studies have addressed the possibility to exploit parasitically OFDM transmitters of communication systems as illuminators of opportunity for PR [8], [9], [10], [11], [12], [13].

It is then interesting to design appropriate signal processing architectures for OFDM radar that allow to perform the typical radar functions while exploiting the peculiar characteristics of such waveforms. As well known, the conventional processing chain of a modern radar includes a disturbance cancellation stage followed by the evaluation of the range-Doppler map [14].

In a continuous wave (CW) radar system, the cancellation stage is devoted to remove the strong direct signal interference as well as multipath clutter returns, which otherwise could mask the weak target echoes, hindering their detection. It is generally performed with adaptive filtering algorithms, which have to take into account both the exploited waveform and the disturbance characteristics and typically require a non-negligible computational effort. Some examples used in PR are [15], [16], [17], [18], and [19].

The evaluation of the range-Doppler map for the area of interest is performed by computing the cross ambiguity function (CAF) between the surveillance signal and the reference signal, namely a copy of the transmitted signal. Ideally, the CAF is equivalent to a bank of matched filters (MF) tuned to different Doppler frequencies. For OFDM signals, this operation presents two major issues.

First, the direct implementation of the CAF is computationally expensive and often unfeasible in real-time applications, due to the typical wide bandwidth of OFDM signals and the long coherent integration times (CITs) generally required to obtain acceptable signal-to-noise ratio (SNR) values. To overcome this issue, suboptimal implementations

based on a batch processing operation are usually employed [8], [20], [21].

Second, the OFDM signal periodical structures, such as pilot carriers, guard intervals, and cyclic prefix (CP), result in an ambiguity function characterized by side-peaks and a high sidelobe floor, which could potentially mask weak targets and increase the false alarm rate. To overcome this problem, multiple solutions were proposed [11], [13], [22]. Among them, the use of reciprocal filter (RF) proved to be an effective alternative to the MF [21], [22], [23], [24], [25], [26], [27], [28], [29], [30], [31], [32]. The RF is applied at the range-compression stage in conjunction with a batch algorithm for CAF evaluation. Specifically, the signal is fragmented into batches corresponding to individual OFDM symbols and the CP is removed. Then, each subcarrier of the surveillance signal is divided by the corresponding subcarrier of the reference signal. As a result, the range-compressed signal presents an equalized spectral response, being independent of the modulation and data content.

The use of this RF-batch approach has two main consequences. On one hand, the signal resulting at the output of the range compression stage has a sinc-shaped response to a point-like target. Therefore, the undesired side-peaks are removed from the range-Doppler map, and the sidelobe floor level is significantly reduced compared to the MF case. Since the RF is a mismatched filter, these advantages are obtained at the expense of a limited and predictable loss, which depends on the data constellation used by the modulation scheme [23], [25]. However, thanks to the lower sidelobe floor, the RF typically outperforms the MF against clutter-limited scenarios [21], [22], [23], [24], [25], [26], [27], [28].

On the other hand, the RF provides a time-invariant and data-independent response to a stationary scatterer. This normalization property can be fruitfully exploited to significantly simplify the disturbance cancellation stage.

In this article, we take this perspective and we deepen the understanding of the RF properties with particular reference to their impact on the disturbance cancellation stage. The idea of leveraging the data-independent output provided by the RF has been mentioned in previous articles [25], [26], [28], [29], where nonadaptive approaches were shown to be applicable similar to the conventional moving target indication (MTI) methodologies from pulsed active radar. In this article, the study is extended to the case of adaptive cancellation schemes, such as those of the various Extensive Cancellation Algorithm (ECA) versions [15], [16], [17], [18], [19]. We show that the computational load of such schemes can be significantly reduced by exploiting the data-independent response of the RF to a point-like target, provided that the output of the range compression stage is fed as input to the disturbance cancellation.

By exploiting this understanding, we look for synergies between different processing stages with the aim to improve the performance of the system while keeping limited its complexity. Specifically, in order to leverage the observed properties of the RF, we propose an alternative, low-complexity processing architecture where the disturbance cancellation is performed downstream of the range compression stage based on the RF. Notice that this is not an obvious approach in CW radar systems using a random waveform, such as, for example, PR [8], [15], [16], [17], [18], [19], where the disturbance cancellation is typically implemented as the first stage. An attempt toward this direction was made in [28] where the proposed architecture was applied against WiFi signals. However, in that case, no specific assumption was made about the signal modulation scheme. In this article, we show that, when operating against OFDM waveforms with batches of length equal to the OFDM symbol, the cascade of RF-based range compression and adaptive cancellation results in a number of additional advantages with respect to those identified in [28]. In fact, the normalization with respect to the structure and the information content of the exploited waveform, provided by the initial application of the RF compression, allows the adaptive cancellation algorithms to deal only with the disturbance characteristics due to the scatterers present in the illuminated area. This results in a significant reduction in the computational cost of conventional adaptive cancellation techniques, without any appreciable performance loss with respect to the original architecture.

Consequently, different solutions are investigated for the technique to be used at the cancellation stage and this provides following additional results that represent further contributions of this article:

1) The consideration of this alternative architectural approach with cancellation applied after range compression, instead of after it, allows interesting interpretations of other existing solutions that apparently do not follow the proposed architectural scheme. Specifically, we show that the Chad scheme, and approaches along that family [23], [24], is equivalent to the cascade of an RF-based range compression stage followed by an ECA-Carriers (ECA-C) approach [18] applied against the range-compressed output. This interpretation within a unique framework has not been considered in previous articles and allows to comparatively assess the advantages and drawbacks of the Chad approach with respect to other solutions.
2) The second consequence of the article is the definition of two alternative processing schemes that leverage the findings above by optimizing either the robustness against severe clutter returns or the computational complexity. In particular, we consider the following conditions:

a) The cascade of an RF-based range compression followed by an adaptive cancellation technique, referred to as ECA-CS (extensive cancellation algorithm by carrier with sliding batches), which greatly benefits from the proposed processing architecture in terms of computational cost reduction and proves to be particularly effective in removing disturbance with a significant internal clutter motion (ICM). Whereas it can be interpreted as a new version from

the family of ECA algorithms, to the best of our knowledge, the proposed ECA-CS approach has not been considered in the technical literature. This is possibly due to the high computational complexity that makes it not feasible for practical applications when it is applied as a first processing stage within the processing architecture. We can resort to such a technique since we use it after the RF-based range compression which makes its cost affordable.

b) The cascade of an RF-based range compression followed single-canceller (SC) MTI approach. As previously mentioned, the idea of leveraging the data-independent output provided by the RF to implement an MTI-like cancellation has been already considered in technical literature. Specifically, this approach has been successfully exploited to enable space-time clutter suppression algorithms, such as DPCA, in PR systems mounted on moving platforms, [25], [26]. In this article, the same concept is extended also to the case of stationary OFDM radar systems and presented as a further simplification of the proposed signal processing architecture, which allows for its performance and computational cost to be compared to other solutions exploiting adaptive cancellation schemes. Along the line of [28], a scheme based on an SC approach is proposed as an extremely simple solution, suitable for clutter scenarios with limited ICM.

The article reports a throughout comparison of alternative architectures encompassing different processing techniques under different clutter conditions, there including the presence of ICM affecting the cancellation stage. Also, the computational complexity is comparatively assessed to offer a complete picture to the interested reader. Finally, the effectiveness of the proposed processing schemes is demonstrated when applied against experimental data. To this purpose, the case of a PR is considered based on OFDM transmissions of opportunity.

The rest of the article is organized as follows. Section II briefly recalls the essential processing stages of a radar exploiting OFDM waveforms and introduces the adopted formalism. A low-complexity processing architecture that applies the disturbance cancellation after a range compression stage based on the RF is proposed in Section III. In Section IV, the ECA-CS and SC approaches are proposed as two alternative disturbance cancellation techniques, with complementary characteristics. A detailed comparison of the considered algorithms, in terms of cancellation performance and computational cost, is then conducted in Section V. In Section VI, the results obtained are verified against experimental data from a passive receiver exploiting a DVB-T signal as illuminator of opportunity. Finally, Section VI concludes this article.

II. OFDM SYMBOL BASED RADAR PROCESSING

We assume that the OFDM-based radar receiver collects a surveillance signal $s[n]$ including the echoes from the area of interest. In addition, it has access to a reference signal $r[n]$, namely a replica of the transmitted signal. The latter is written as a sequence of P OFDM symbols, being each symbol composed of N_U useful samples and a CP of N_{CP} samples

$$r[n] = \sum_{p=0}^{P-1} w_{N_S}\left[n - pN_S\right] \sum_{k=0}^{N_U-1} R_{pk} e^{\frac{j2\pi k(l-N_{CP}-pN_S)}{N_U}}. \quad (1)$$

In (1), R_{pk} represent the complex value transmitted at the kth subcarrier for the pth OFDM symbol, whereas $w_{N_S}[n]$ is a time-windowing function of duration $N_S = N_{CP} + N_U$ samples, which extends the subsequent N_U-points Discrete Fourier Transform (DFT) output over the entire OFDM symbol duration.

The surveillance signal is written as the superposition of contributions due to the direct signal coming from the transmitter, the clutter/multipath echoes from the stationary scene, moving targets' echoes, and thermal noise

$$s[n] = \gamma_0 r[n] + \sum_{m=1}^{M_C-1} \gamma_m r[n - \bar{n}_m] + \sum_{m=0}^{M_T-1} \delta_m r[n - \tilde{n}_m] e^{\frac{j2\pi n f_m}{N_U \Delta f}} + d[n] \quad (2)$$

where

1) γ_0, γ_m, and δ_m are the amplitudes of the direct signal, the mth clutter/multipath echo, and the mth target echo at the surveillance channel, respectively, relative to the reference channel; they will be assumed constant within the CIT in the absence of ICM, whereas a random temporal variability could be considered for clutter returns affected by ICM according to a Gaussian power spectral model;
2) $\bar{n}_m$ and $\tilde{n}_m$ are the delays associated to the mth stationary or moving scatterer echo;
3) f_m is the Doppler frequency associated to the mth moving target echo being Δf the subcarrier spacing; and
4) $d[n]$ is the additive white Gaussian noise contribution (AWGN).

In the following, we assume that the OFDM frame start has been identified and the surveillance and reference signal have been synchronized in a preprocessing stage. Correspondingly, let us define S_{pk} as the complex values obtained at the kth subcarrier of the pth OFDM symbol for the surveillance signal, after removing the CP and applying a DFT over the useful OFDM symbol portion

$$S_{pk} = \sum_{l=0}^{N_U-1} s\left[l + pN_S\right] e^{-\frac{j2\pi kl}{N_U}}. \quad (3)$$

As previously mentioned, the essential steps prior to target detection are the cancellation of the disturbance and the evaluation of the range-Doppler map. The range-Doppler map is obtained by computing the CAF between the surveillance signal $s[n]$ and the reference signal $r[n]$. Before

this stage, a disturbance cancellation stage is generally required to remove the undesired contributions from the surveillance signal, i.e., direct signal interference and the clutter/multipath echoes, which may severely hinder the detection of targets.

In the following, the main signal processing stages are described with reference to the use of OFDM signals, highlighting the typical processing methods used to mitigate the impact of the OFDM waveform characteristics on the radar performance.

A. Disturbance Cancellation

Several disturbance cancellation algorithms have been proposed to remove the direct signal interference and the clutter echoes. Some examples for PR are introduced in [15] and [19]. Among them, the ECA has proven to be an effective and robust solution for multiple scenarios and illuminators of opportunity [15]. The ECA resorts to a least-square approach to minimize the disturbance output power by projecting the surveillance signal into a subspace orthogonal to the disturbance subspace. Basically, the disturbance signal is estimated by means of weighted delayed and Doppler-shifted replicas of the reference signal, and then subtracted from the surveillance signal. The main drawback of the ECA is that it generally requires a high computational load, which has motivated the introduction of various modifications of the algorithm, aimed at speeding-up its implementation [16], [18], [19].

In particular, the ECA-C [18] is specifically tailored for the case of OFDM waveforms. Exploiting the OFDM signal structure, this algorithm operates in the frequency domain on a subcarrier basis, considerably reducing the computational cost compared to the original ECA.

The ECA-C operation for each subcarrier k can be described as

$$\boldsymbol{S}_k^{\mathrm{ECA-C}} = \boldsymbol{S}_k - \alpha_k \boldsymbol{R}_k \tag{4}$$

where $\boldsymbol{S}_k$ and $\boldsymbol{R}_k$ are vectors of dimension $P \times 1$ that collect the values S_{pk} and R_{pk} for all the P OFDM symbols in the CIT, and $\boldsymbol{S}_k^{\mathrm{ECA-C}} = [S_{0k}^{\mathrm{ECA-C}}\ S_{1k}^{\mathrm{ECA-C}}\ \ldots\ S_{P-1\,k}^{\mathrm{ECA-C}}]^T$ represents the disturbance-free version of the surveillance signal at the kth carrier arranged as $\boldsymbol{S}_k$. The cancellation coefficient α_k is adaptively selected so as to minimize the signal power at the corresponding subcarrier at the output of the cancellation stage

$$\alpha_k = \underset{\alpha}{\operatorname{argmin}} \left\{ \|\boldsymbol{S}_k^{\mathrm{ECA-C}}\|^2 \right\} = \frac{\boldsymbol{R}_k^H \boldsymbol{S}_k}{|\boldsymbol{R}_k|^2} = \frac{\sum_{b=0}^{P-1} S_{bk} R_{bk}^*}{\sum_{t=0}^{P-1} |R_{tk}|^2}. \tag{5}$$

B. Range-Doppler Map Evaluation

After disturbance cancellation is performed, the range-Doppler map is obtained by computing the CAF between the ideally disturbance-free surveillance signal and the reference signal. The evaluation of the CAF might be computationally expensive, especially when exploiting wide bandwidth signals. Therefore, in practical applications, suboptimal implementations based on batch processing architectures are typically used [8], [20]. These allow to approximate the ideal CAF, while possibly enabling the real-time operation.

When an OFDM signal is exploited, the typical implementation of the suboptimal batch algorithm uses a length of the batches equal to the useful part of the OFDM symbols, after the removal of the CP. The effect of the Doppler frequency is neglected within each batch, where a zero-Doppler range compression is performed. Then, a DFT coherently integrates the results from consecutive batches within the CIT. The resulting range-Doppler map $z[l, m]$ at the generic lth range bin and mth Doppler bin is obtained as

$$z[l, m] \cong \frac{1}{L} \sum_{p=0}^{P-1} e^{-\frac{j2\pi mp}{P}} \sum_{k=0}^{L-1} X_{pk} H_{pk} e^{\frac{j2\pi kl}{L}} \tag{6}$$

where

1) L is the number of nonzero subcarriers in the OFDM symbol;
2) X_{pk} is the surveillance signal at the output of the cancellation stage, i.e., $X_{pk} = S_{pk}^{\mathrm{ECA-C}}$; and
3) H_{pk} is the range compression filter at the pth batch and the kth subcarrier.

In addition, we recognize the inner summation $\chi_{pl} = \sum_{k=0}^{L-1} X_{pk} H_{pk} e^{\frac{j2\pi kl}{L}}$, which implements the range compression in the frequency domain, on a symbol-by-symbol basis.

A conventional range compression filter is the MF, which guarantees the best performance in terms of SNR. However, when applied to OFDM waveforms of opportunity, the MF may produce a range-Doppler map characterized by a relatively high random sidelobe floor and undesired side peaks [13]. This is due to the variable data content and periodical structures in the employed signal—namely pilot carriers, guard intervals, and CP—inserted to aid the communication function, addressing issues, such as synchronization, channel distortions, and multipath propagation. To control the undesirable effects on the waveform ambiguity function, an attractive mismatched filtering strategy can be used for range compression, exploiting the RF. The corresponding expressions of the two filters are specified as

$$H_p[k] = \begin{cases} R_{pk}^* & MF \\ \frac{1}{R_{pk}} & RF. \end{cases} \tag{7}$$

To illustrate the differences between the MF and RF, let us consider a point-like target at range-Doppler bin $[l_0, m_0]$. If the surveillance signal contains only the echo from the target, the input to the range compression is written as

$$x[n] = \delta_0 r[n - l_0]\, e^{\frac{j2\pi n f_0}{N_U \Delta f}} \tag{8}$$

being $f_0 = \frac{m_0 N_U \Delta f}{P N_S}$. Assuming that the delay of the target echo is smaller than the CP, i.e., $\tilde{n}_0 < N_{\mathrm{CP}}$, and the Doppler

induced phase shift within each OFDM symbol is negligible, the complex values obtained at the kth subcarrier of the pth OFDM symbol for the surveillance signal, after removing the CP and applying a DFT over the useful OFDM symbol portion, can be approximated as

$$X_{pk} = \delta_0 R_{pk} e^{\frac{j2\pi pm_0}{P}} e^{-\frac{j2\pi kl_0}{L}}. \tag{9}$$

Using the definitions in (7), the range compressed signal χ_{pl} results in

$$\chi_{pl} = \begin{cases} \delta_0 e^{\frac{j2\pi pm_0}{P}} \sum_{k=0}^{L-1} |R_{pk}|^2 e^{\frac{j2\pi k(l-l_0)}{L}} & MF \\ \delta_0 e^{\frac{j2\pi pm_0}{P}} \sum_{k=0}^{L-1} e^{\frac{j2\pi k(l-l_0)}{L}} & RF \end{cases} \tag{10}$$

where it is evident that, while the MF response depends on the content encoded in the OFDM symbols subcarriers R_{pk}, the RF produces a deterministic sinc-like response, as it normalizes the signal with respect to the structure and information content of the waveform.

This RF feature yields two main advantages. First, it effectively mitigates the undesired characteristics of the signal ambiguity function, namely the high sidelobes and side-peaks, providing a perfectly whitened response. This is obtained at the expense of a limited and predictable SNR loss with respect to the MF, depending on the OFDM constellation [23], [25]. Still the lower sidelobe response in the range-Doppler domain allows the RF to outperform the MF against clutter-limited scenarios [21], [22], [23], [24], [25], [26], [27], [28].

Second, it makes data-independent the response to a point-like target, thus providing a time-invariant output after the range compression stage. This can play a fundamental role in simplifying the disturbance cancellation stage if the typical processing architecture is changed and the cancellation stage is cascaded to the range compression stage. In principle, this enables the application of simple nonadaptive clutter cancellation solutions, borrowed from the conventional MTI techniques of pulsed active radar [25], [26], [27], [28]. Moreover, this alternative and low-complexity architecture allows to redefine some of the standard adaptive disturbance cancellation algorithms, by significantly reducing their computational cost.

We recall that the above property applies under the hypotheses made to move from (8) to (9), namely when the delay of the target echo is smaller than the CP duration and its Doppler is negligible. Under different conditions, the considered echo would yield an RF response in the sidelobes region that depends on the specific range and Doppler values of the target. Specifically, as the range and Doppler increase, the RF response progressively deviates from the ideal sinc-shape yielding random sidelobes [21].

However, in this article, we exploit the above characteristic of the RF with the aim to simplify the clutter cancellation stage. In this regard, it is worth noticing that the echoes we are most interested in come from the very first range cells and show a negligible Doppler shift, only due to possible ICM. Therefore, for such echoes, the hypotheses above are largely verified.

III. DISTURBANCE CANCELLATION AFTER RECIPROCAL FILTER

Based on the alternative architecture above, in this section, we analyze the effects of the application of the range compression with an RF on the following disturbance cancellation stage and evaluate the resulting simplifications and cost reduction.

Fig. 1 illustrates the considered processing architectures. In particular, Fig. 1(a) shows the conventional processing stages that applies a generic cancellation algorithm before the range compression, while Fig. 1(b) illustrates the proposed architecture, which performs first the range compression with the RF and then the disturbance removal against range compressed data. To better appreciate the effect of the RF on the subsequent disturbance cancellations stage, it is convenient to conceptually redefine the surveillance and reference signals at the output of the RF range compression

$$\begin{cases} S_{pk}^{\mathrm{RF}} = \frac{S_{pk}}{R_{pk}} \\ R_{pk}^{\mathrm{RF}} = 1 \end{cases} \tag{11}$$

where we assumed that the signal at the input of the range compression is $X_{pk} = S_{pk}$ or $X_{pk} = R_{pk}$, respectively.

As apparent, the RF yields a perfectly whitened reference signal and normalizes the surveillance signal with respect to the exploited waveform. As a result, the subsequent disturbance cancellation stage is only fed with the range-compressed surveillance signal S_{pk}^{RF}, as shown in Fig. 1(b), since it no longer requires information on the content of the exploited waveform.

A. RF+ECA-C for Static Clutter Removal

In order to compare the two processing architectures and interpret the effect of the change in the order of the stages, we consider the ECA-C as disturbance cancellation algorithm, without loss of generality. When the architecture in Fig. 1(a) is adopted, referred to as ECA-C+RF, using (4), (5), and (7), the resulting signal can be obtained as

$$S_{pk}^{\mathrm{ECA-C+RF}} = \frac{S_{pk}}{R_{pk}} - \alpha_k = \frac{S_{pk}}{R_{pk}} - \frac{\sum_{b=0}^{P-1} S_{bk} R_{bk}^*}{\sum_{t=0}^{P-1} |R_{tk}|^2}. \tag{12}$$

On the other hand, when the ECA-C is applied after the RF according to the architecture in Fig. 1(b), referred to as RF+ECA-C, the corresponding cancellation coefficients are estimated to minimize the output power of the range-compressed signal

$$\begin{aligned} \tilde{\alpha}_k &= \underset{\alpha}{\mathrm{argmin}} \left\{ \| \boldsymbol{S}_k^{\mathrm{RF+ECA-C}} \|^2 \right\} \\ &= \frac{\left(\boldsymbol{R}_k^{\mathrm{RF}}\right)^H \boldsymbol{S}_k^{\mathrm{RF}}}{\left|\boldsymbol{R}_k^{RF}\right|^2} = \frac{1}{P} \sum_{b=0}^{P-1} \frac{S_{bk}}{R_{bk}} \end{aligned} \tag{13}$$

which results in

$$S_{pk}^{\mathrm{RF+ECA-C}} = \frac{S_{pk}}{R_{pk}} - \tilde{\alpha}_k = \frac{S_{pk}}{R_{pk}} - \frac{1}{P} \sum_{b=0}^{P-1} \frac{S_{bk}}{R_{bk}}. \tag{14}$$

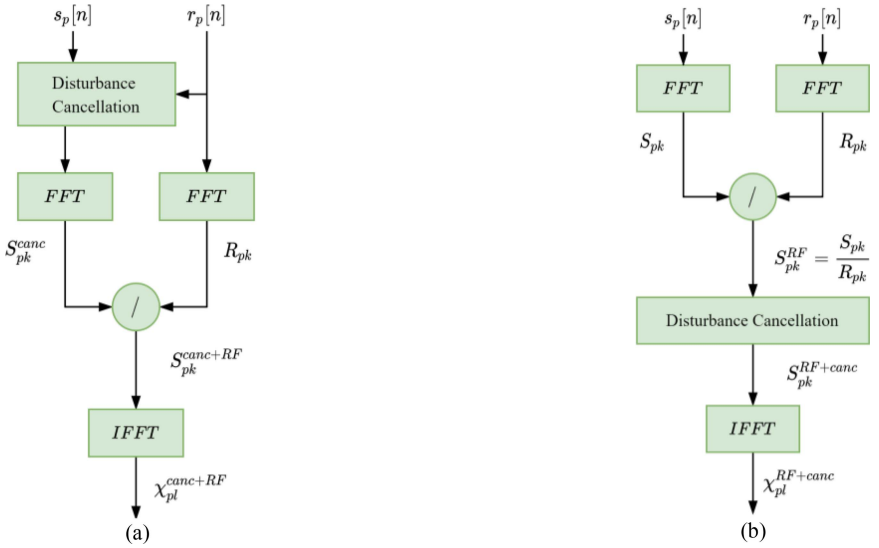

Fig. 1. OFDM-based radar processing schemes. (a) Disturbance cancellation stage followed by range compression with the RF. (b) Range compression with RF followed by disturbance cancellation stage.

Comparing (12) and (14), it appears that the proposed processing architecture is not completely equivalent to the conventional one. In particular, the difference lies in the strategy adopted for the optimization of the cancellation coefficients. In both cases, this is aimed at minimizing the disturbance output power by projecting the corresponding surveillance signal into a subspace orthogonal to the estimated disturbance subspace. However, in the ECA-C+RF scheme, the coefficient α_k is selected such as to minimize the power of the surveillance signal $\boldsymbol{S}_k^{\mathrm{ECA-C}}$at the output of the cancellation stage for each subcarrier. Instead, in the proposed RF+ECA-C scheme, the coefficients $\tilde{\alpha}_k$ are selected to minimize the output power of the range-compressed signal $\boldsymbol{S}_k^{\mathrm{RF+ECA-C}}$ for each subcarrier.

In the case of OFDM signals with QPSK constellation, namely for signals with a constant amplitude spectrum, the two schemes are exactly equivalent. In fact, by substituting into (12), a constant symbol energy $|R_{pk}|^2 = c$, we obtain

$$S_{pk}^{\mathrm{ECA-C+RF}} = \frac{S_{pk}}{R_{pk}} - \frac{1}{Pc}\sum_{b=0}^{P-1}\frac{S_{bk}}{R_{bk}}c = \frac{S_{pk}}{R_{pk}} - \frac{1}{P}\sum_{b=0}^{P-1}\frac{S_{bk}}{R_{bk}} = S_{pk}^{\mathrm{RF+ECA-C}}. \quad (15)$$

Note that similar results could be demonstrated also considering other ECA-based cancellation algorithms.

It is also worth noting that the expression in (14) for the RF+ECA-C scheme is equivalent to the one obtained for the Doppler channel detector with rejection of the zero Doppler contribution (Chad-ZDC), proposed in [23]. In fact, the first term corresponds to the pth channel frequency response as defined in [23], while the second term can be interpreted as the static channel estimation. This demonstrates that the Chad-ZDC is equivalent to applying the ECA-C after an RF-based range compression stage. This finding contributes to unify the existing conceptualizations of the range compression and disturbance cancellation techniques and provides an interesting interpretation of techniques that do not immediately look as following within the considered architecture.

To further analyze the differences between the two processing architectures, Fig. 2 shows the range-Doppler maps obtained with each architecture for a simulated DVB-T 8K signal with a 64QAM constellation. A CIT of 0.7 s was considered for the processing. The simulated surveillance signal contains AWGN, static clutter (i.e., with no ICM) extended up to 8 km bistatic range, and the echoes from two point-like targets, respectively, located at 2 and 5 km bistatic range, moving at 11 and -3.7 m/s bistatic radial velocity (corresponding to 25 and -8 Hz Doppler frequency at the considered carrier frequency). Both the targets are simulated with an SNR $= -40$ dB, measured at the input of the processing chain, while the corresponding clutter-to-noise ratio (CNR) is set to CNR $=$ 10 dB. For comparison purposes, the resulting signal-to-clutter plus noise ratio (SCNR) at the output of the processing chain is indicated on each map close to the relative target location. This is computed by taking the ratio between the target peak power level and the disturbance power, which is estimated by averaging over the map cells in an area around the target indicated by the white rectangles.

As evident, both architectures allow to effectively remove the clutter disturbance and no significant differences between the resulting range-Doppler maps can be noticed, apart from the zero Doppler bin, where the RF+ECA-C scheme shows lower values compared to the ECA-C+RF scheme. Moreover, the two schemes provide the same SCNR for both the considered targets, thus offering comparable detection capabilities in the considered example.

On the other hand, the RF+ECA-C scheme enables a significant reduction of the computational load required

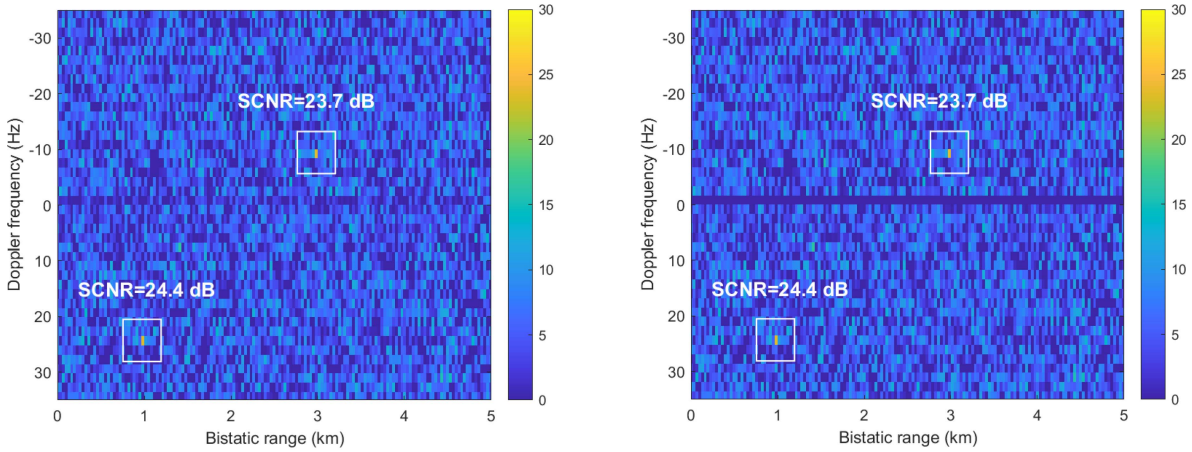

Fig. 2. Range-Doppler maps obtained for a simulated clutter scenario including two targets and no ICM. (a) Exploiting the ECA-C + RF scheme. (b) Exploiting the RF + ECA-C scheme. A simulated DVB-T signal is assumed as a reference signal.

TABLE I
Number of Operations Required by Each Cancellation Algorithm Applied Before and After the RF

Algorithm	Application	Expression	# Complex Multiplications	# Complex Additions	# FLOPS (6CM+2CA)
ECA-C	Conventional (before range compression)	$S_{pk} - \left(\frac{\sum_{b=0}^{\mathrm{P}-1} R_{bk}^{*} S_{bk}}{\sum_{t=0}^{\mathrm{P}-1} \lvert R_{tk}\rvert^2}\right) R_{pk}$	$3PL$	$3PL$	$24PL$
	After RF	$S_{pk}^{RF} - \frac{1}{P}\sum_{b=0}^{P-1} S_{bk}^{RF}$	L	$2PL$	$L(6+4P)$
ECA-CD	Conventional (before range compression)	$\boldsymbol{S}_k - \boldsymbol{Q}_k(\boldsymbol{Q}_k^H\boldsymbol{Q}_k)^{-1}\boldsymbol{Q}_k^H\boldsymbol{S}_k$	$L\left(\frac{1}{2}W^3+\frac{5}{2}W^2+W^2P+2WP\right)$	$L\left(\frac{1}{2}W^3+\frac{1}{2}W^2+W^2P+2WP+P\right)$	$L\left(4W^3+16W^2+8W^2P+16WP+2P\right)$
	After RF	$\boldsymbol{S}_k^{RF} - \boldsymbol{P}\boldsymbol{S}_k^{RF}$	$L(2WP)$	$L(2WP+P)$	$L(16WP+2P)$
ECA-CS	Conventional (before range compression)	$S_{pk}^{ECA-CS} = S_{pk} - \alpha_k^s R_{pk}$	$PL\left(3+\frac{1}{N_b}\right)$	$PL\left(3+\frac{4}{N_b}\right)$	$PL\left(24+\frac{14}{N_b}\right)$
	After RF	$S_{pk}^{RF} - \frac{1}{N_s}\sum_{t=p_c-N_s/2}^{p_c+N_s/2-1} S_{tk}^{RF}$	PL/N_b	$PL\left(2+\frac{2}{N_b}\right)$	$PL\left(4+\frac{10}{N_b}\right)$
SC	After RF	$\chi_{pl}^{RF} - \chi_{(p-\mathrm{D})l}^{RF+SC}$	0	PL	$2PL$

by the disturbance cancellation stage. This is evident by comparing the expressions for computing the cancellation coefficients in (5) and (13). While the estimation of the coefficients α_k in the ECA-C+RF scheme requires multiple complex multiplications (CM) and sums, the coefficients $\tilde{\alpha}_k$ in the RF+ECA-C scheme are computed by simply evaluating the mean over P symbols for the kth subcarrier of the range-compressed signal $\boldsymbol{S}_k^{\mathrm{RF}}$.

To quantify the computational cost reduction, Table I displays the CM and complex additions (CA) required by the ECA-C when applied before and after the RF (see first two rows of Table I). As expected, the number of required operations is greatly reduced in the RF+ECA-C scheme. In particular, the CM becomes independent of the number of OFDM symbols P, which results in a great advantage in terms of computational load compared to the conventional architecture, especially when longer CIT are exploited.

B. RF+ECA-CD for Clutter With ICM

As known, while the ECA-C is effective in removing static disturbance, its cancellation capability is reduced when applied to clutter with ICM. To overcome this limitation, an enhanced version of the ECA-C was proposed in [19], referred to as ECA-Carrier and Doppler (ECA-CD). It expands the clutter subspace on Doppler-shifted replicas of the reference carriers. Specifically, q symmetric replicas

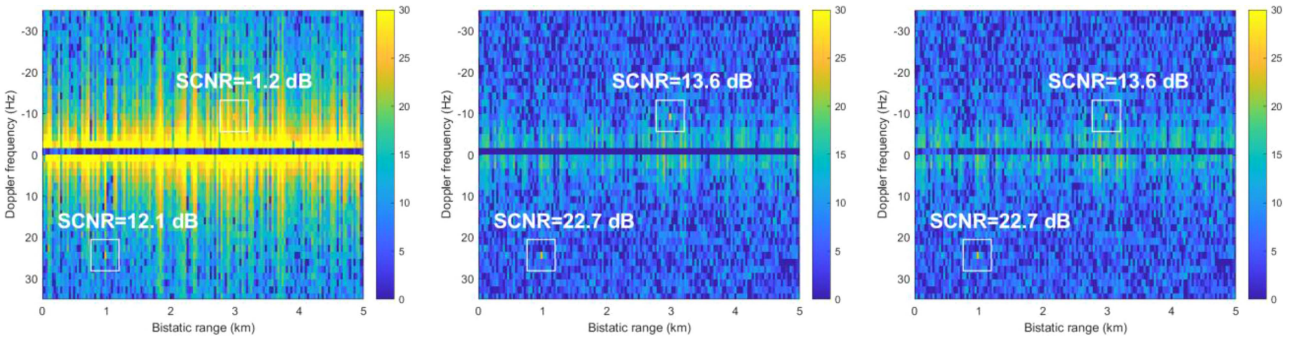

Fig. 3. Range-Doppler maps obtained for a simulated clutter scenario including two targets and strong ICM ($\sigma_v = 0.1$ m/s): exploiting (a) RF+ECA-C; (b) RF + ECA-CD; and (c) ECA-CD + RF.

evenly spaced in Doppler by δf are considered. Therefore, the ECA-CD provides a wider cancellation notch with respect to the ECA-C, resulting in a better cancellation performance in scenarios affected by ICM. Its operation can be described as

$$\boldsymbol{S}_k^{\mathrm{ECA-CD}} = \boldsymbol{S}_k - \boldsymbol{P}_k \boldsymbol{S}_k = \boldsymbol{S}_k - \boldsymbol{Q}_k \left(\boldsymbol{Q}_k^H \boldsymbol{Q}_k\right)^{-1} \boldsymbol{Q}_k^H \boldsymbol{S}_k \quad (16)$$

where $\boldsymbol{P}_k$ represents the clutter subspace projection matrix and $\boldsymbol{Q}_k$ is a $P \times W$ matrix with $W = 2q + 1$, obtained as

$$\boldsymbol{Q}_k = \left[\left(\boldsymbol{\Lambda}^q\right)^H \boldsymbol{R}_k \ldots \boldsymbol{\Lambda}^H \boldsymbol{R}_k,\ \boldsymbol{R}_k,\ \boldsymbol{\Lambda} \boldsymbol{R}_k \ldots \boldsymbol{\Lambda}^q \boldsymbol{R}_k\right]_{P \times W} \quad (17)$$

where $\boldsymbol{\Lambda}^b = \mathrm{diag}\{1, e^{j2\pi b \delta f T_S}, \ldots, e^{j2\pi (P-1) b \delta f T_S}\}$ is a phase-shifting diagonal matrix where T_S is the OFDM symbol duration.

Fig. 3 shows the range-Doppler maps obtained with the ECA-CD applied before [Fig. 3(c)] and after [Fig. 3(b)] the RF. The results of the RF+ECA-C scheme are also reported for comparison [Fig. 3(a)]. The same scenario of Fig. 2 is considered with the difference that in this case the clutter is affected by ICM. Specifically, clutter returns are modeled with a Gaussian power spectrum centred in zero Doppler and with an rms spectral width $\sigma_v = 0.1$ m/s. The ECA-CD uses $q = 1$ symmetric reference signal replica shifted at ± 0.84 Hz.

As expected, in Fig. 3(a), the ECA-C fails to effectively suppress the clutter, and the residuals significantly degrade the targets SCNR, with respect to the case of no ICM shown in Fig. 2(b). In particular, the SCNR of the target closer to zero Doppler suffers a higher degradation as it is totally masked by the clutter residuals. Conversely, the ECA-CD yields an improved clutter suppression, since the cancellation notch is extended with respect to the ECA-C, resulting in higher SCNR values. Since the clutter residuals are not completely removed, the SCNR for the target closer to zero Doppler is still much lower than the one obtained in the absence of ICM. This suggests the need to consider additional symmetric replicas for the clutter subspace to extend the cancellation notch, which would result in increased complexity.

In fact, the flexibility and improved cancellation capability of ECA-CD is paid with a higher computational cost. From (16), it is evident that the ECA-CD involves a matrix inversion and several complex matrix-vector multiplications, which significantly increase the required number of operations with respect to the ECA-C.

This cost can be greatly reduced when the ECA-CD is applied after range compression with the RF. Moreover, comparing the maps in Fig. 3(b) and (c), it is apparent that the ECA-CD cancellation performance remains almost unchanged when applied with the proposed architecture.

The computational cost reduction can be measured by recognizing that after the range compression with the RF, the reference signal vector for each subcarrier becomes a vector of ones, i.e., $\boldsymbol{R}_k = 1_{P \times 1}$, regardless of the data content. Therefore, the disturbance subspace projection matrix $\boldsymbol{P}_k = \boldsymbol{P}$ is constant for each subcarrier and can be precomputed, since independent of the exploited signal, significantly reducing the number of operations required by the ECA-CD. Given the a-priori known projection matrix $\boldsymbol{P}$, the ECA-CD is simplified to

$$\boldsymbol{S}_k^{\mathrm{RF+ECA-CD}} = \boldsymbol{S}_k^{\mathrm{RF}} - \boldsymbol{P} \boldsymbol{S}_k^{\mathrm{RF}}. \quad (18)$$

Table I displays the number of operations required by the ECA-CD when applied using the considered processing architectures. As expected, when the ECA-CD is performed after the RF, there is a significant reduction in the number of CM and CA compared to the conventional application.

IV. ALTERNATIVE CANCELLATION TECHNIQUES

Generally, the disturbance cancellation stage presents a tradeoff between effectiveness of the disturbance removal and required computational cost. In this section, we propose two alternative cancellation strategies, which benefit from the proposed processing architecture and individually meet the two opposing requirements. On one hand, an SC approach is considered, which exploits the data-independent and time-invariant response at the output of the RF-based range compression to perform a nonadaptive cancellation with a minimal computational cost, suitable for relatively static clutter scenarios. On the other hand, we introduce a sliding version of the ECA-C algorithm, referred to as ECA-CS, which provides instead a great flexibility and

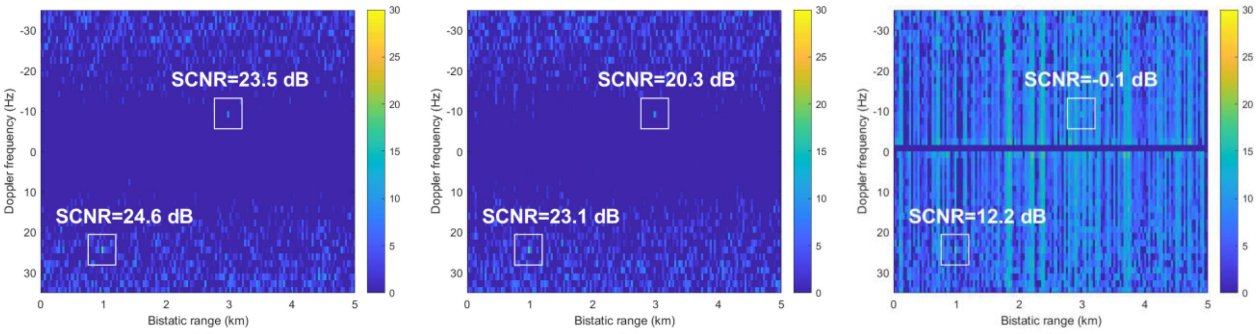

Fig. 4. Range-Doppler map obtained with the RF + SC scheme for a simulated clutter scenario (a) in the absence of ICM; (b) with weak ICM ($\sigma_v = 0.01$ m/s); and (c) with strong ICM ($\sigma_v = 0.1$ m/s).

improved robustness against ICM, at the expense of a higher computational load.

A. Single Canceller (SC)

Besides providing a significant simplification of the adaptive cancellation techniques, the preliminary range compression with an RF also enables the adoption of simple cancellation approaches based on the nonadaptive subtraction of delayed portions of the surveillance signal, similar to those used in MTI pulsed radar systems, provided that the variability due to ICM is negligible within the observation time.

As shown in (10), the range-compressed signal at the output of the RF χ_{pl}^{RF} is independent of the data-content, providing a time-invariant response to a point-like target echo. In fact, for direct signal and static clutter contributions ($m_0 = 0$), χ_{pl}^{RF} is independent of the symbol index p. As a result, a simple nonadaptive disturbance cancellation could be achieved by subtracting different portions of the signal, delayed by D OFDM symbols $\chi_{(p-D)l}^{\mathrm{RF}}$ [28]. The clutter cancellation is obtained as

$$\chi_{pl}^{\mathrm{RF+SC}} = \chi_{pl}^{\mathrm{RF}} - \chi_{(p-D)l}^{\mathrm{RF}}. \tag{19}$$

This method resembles the approach typically used for disturbance removal in active MTI radar systems, based on the transmission of a train of identical pulses. From (19), it is clear that the SC is very efficient in terms of computational resources. In fact, it achieves the cancellation by subtracting a delayed replica of the range-compressed signal and does not require any CM, as shown in Table I. This makes the SC the fastest cancellation technique analysed so far. Similar considerations apply to the more general case of nonadaptive cancellation filters with multiple taps, as for example the binomial cancelers [27].

Fig. 4(a) shows the range-Doppler map obtained using the RF+SC scheme applied in the case of a completely static disturbance (no ICM). As evident, the SC achieves an effective cancellation of the clutter returns, enabling the detection of both targets with performance comparable to the ECA-C case in Fig. 2.

On the other hand, Fig. 4(b) displays the map resulting from the application of the RF+SC scheme against clutter affected by a weak ICM level, characterized by an rms spectral width $\sigma_v = 0.01$ m/s. Although the SC still effectively removes the disturbance, the resulting target SCNR values are slightly lower compared to the previous case, especially for the slower target. This degradation is expected to increase as the ICM level increases.

This is illustrated in Fig. 4(c), which shows the map obtained when the RF+SC scheme is applied in a relatively strong ICM condition ($\sigma_v = 0.1$ m/s). As apparent, a significant clutter suppression is achieved compared to that obtained with the RF+ECA-C scheme in Fig. 3(a), where the same ICM level was considered. However, non-negligible clutter residuals are present, resulting in low SCNR values and a reduced detection capability also when compared to the results in Fig. 3(b) and (c). This is especially true for the slower target, which suffers a higher SCNR loss compared to the faster target.

In principle, the width of the cancellation notch can be controlled by varying the delay, namely the number of delayed symbols D. A shorter delay will result in a wider cancellation notch [28]. However, the cancellation does not discriminate between target and clutter echoes. Therefore, while an extended cancellation notch could more effectively tackle the ICM, it would also suppress the slower targets, resulting in a good detection performance only for faster targets.

Basically, the SC solution is able to perfectly remove the clutter assuming that the disturbance returns are time-invariant after the range compression with the RF, which removes the variability associated to the exploited signal. While this condition is ideally satisfied in the absence of ICM, in practical cases the clutter returns are Doppler-spread and variable in time. This variability increases with the level of ICM and may reduce the cancellation performance of the SC approach, as in the case of Fig. 4(c). Nevertheless, in clutter scenarios characterized by a negligible ICM (or in applications where we are interested in sufficiently fast targets), the SC offers a satisfactory performance, with a much lower computational complexity compared to the adaptive cancellation techniques. In

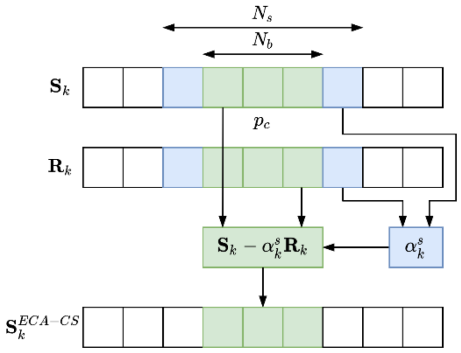

Fig. 5. Sketch of the ECA-CS flow diagram.

addition, we notice that this approach does not require any matrix inversion so that it could be easily implemented on simple processing hardware architectures.

B. ECA-C With Sliding Batches (ECA-CS)

To effectively suppress a clutter affected by a significant ICM, several techniques have been proposed for PR exploiting a generic waveform of opportunity. In particular, the ECA-sliding (ECA-S) technique, presented in [16], operates by applying ECA to a sliding portion (batch) of the signal and estimating the cancellation coefficients over an extended batch. This offers the possibility to widen the cancellation notch compared to the original ECA, resulting in an improved performance when operating against ICM, at the expense of a higher overall computational complexity.

Inspired by this concept, we consider the use of the ECA-C algorithm, which is specifically designed for OFDM-based PR, exploiting a sliding batch strategy. We refer to this approach as ECA-CS. In Fig. 5, we illustrate the ECA-CS operation for a generic signal subcarrier k. The cancellation coefficient α_k^s for the current batch is estimated over N_s symbols centred around the batch

$$\alpha_k^s = \frac{\sum_{b=p_c-N_s/2}^{p_c+N_s/2} R_{bk}^* S_{bk}}{\sum_{t=p_c-N_s/2}^{p_c+N_s/2} |R_{tk}|^2} \tag{20}$$

where p_c denotes the central symbol index of the current batch including N_b symbols. The cancellation is then applied only to the symbols within the batch, resulting in

$$S_{pk}^{\mathrm{ECA-CS}} = S_{pk} - \alpha_k^s R_{pk} \quad \forall p_c - \frac{N_b}{2} < p < p_c + \frac{N_b}{2}. \tag{21}$$

As for the ECA-S, the width of the cancellation notch can be extended by selecting $N_s < P$, thus sensibly enhancing the performance against ICM. Apparently, this improvement is paid with a higher computational load. As evident from (20) and (21), the evaluation of the cancellation coefficients is performed multiple times over consecutive (partially overlapped) batches, resulting in a much higher number of operations compared to standard ECA-C.

However, when the ECA-CS is applied after the RF, using the architecture suggested in Fig. 1(b), its computational complexity can be considerably reduced. By substituting (11) into (21), similarly to the result obtained in (14) for the ECA-C case, we obtain

$$S_{pk}^{\mathrm{RF+ECA-CS}}[k] = \frac{S_{pk}}{R_{pk}} - \frac{1}{N_s} \sum_{b=p_c-\frac{N_s}{2}}^{p_c+\frac{N_s}{2}} \frac{S_{bk}}{R_{bk}} \quad \forall p_c - \frac{N_b}{2} < p < p_c + \frac{N_b}{2}. \tag{22}$$

Likewise, the operation for a given batch is simplified to the subtraction of the mean value of the signal portion used to estimate the cancellation coefficient. From (22), we note that the ECA-C represents a particular case of the ECA-CS, where $N_b = N_s = P$, namely the number of OFDM symbols in the CIT.

Table I shows the number of operations required by the ECA-CS when applied before and after the RF. A naive implementation of the ECA-CS would led to recompute the cancellation coefficients many times for each overlapping portion of N_b samples. Instead, we use an efficient sliding implementation in which a cumulative vector sum is applied first so that, for each N_b samples, the update of the coefficients requires much fewer operations. This implementation impacts the application of the ECA-CS both before and after the RF and the number of operations in Table I are reported assuming this implementation. Still we notice that when the ECA-CS is used after the RF, a further reduction of the computational cost is obtained. Obviously, when the ECA-CS is applied with $N_s = N_b = P$, the number of CM and CA reduces to the values of the ECA-C.

Fig. 6 shows the range-Doppler map obtained when applying the RF+ECA-CS to the same clutter scenario considered in Figs. 3 and 4(c). The batch length is set to $N_b = 3$, while the length of the portion used to compute the estimation coefficient is $N_s = P/6$. As clearly visible in the map, the resulting wider cancellation notch allows to effectively remove the disturbance affected by ICM. The resulting SCNR values for the considered targets are higher than those obtained with the ECA-C and ECA-CD.

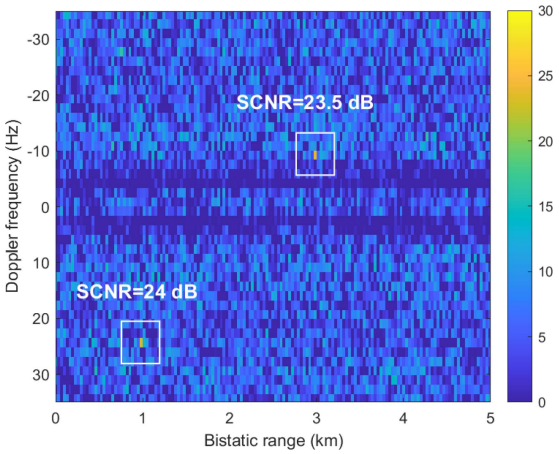

Fig. 6. Range-Doppler map obtained with the RF+ECA-CS scheme for a simulated clutter scenario in the presence of ICM.

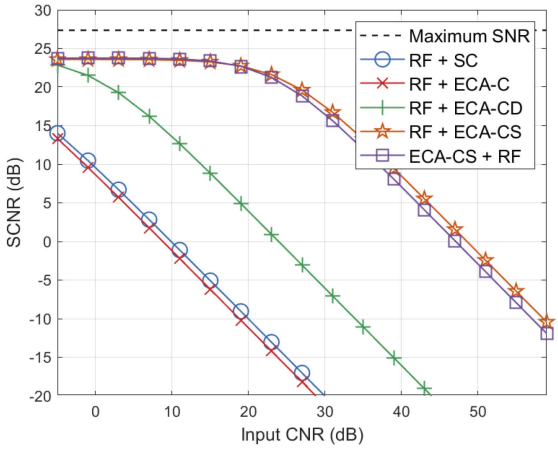

Fig. 7. Achievable SCNR for a point-like target as a function of the input CNR for each cancellation technique applied to a simulated clutter scenario in the presence of ICM.

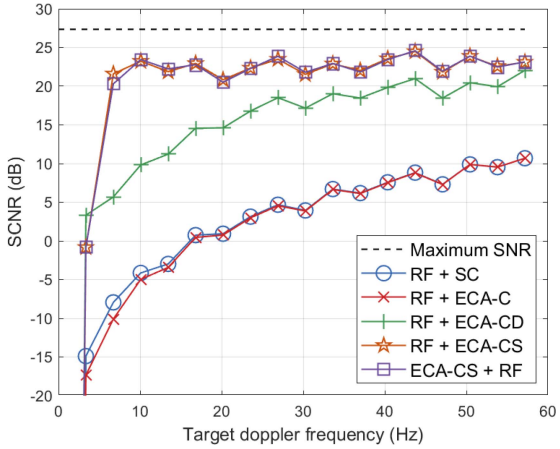

Fig. 8. Achievable SCNR for a point-like target as a function of the target Doppler frequency for each cancellation technique applied to a simulated clutter scenario in the presence of ICM.

Moreover, also the SCNR of the slower target is comparable to the case with no ICM in Fig. 2(b), which implies that the ECA-CS achieves an almost complete suppression of the clutter in the considered example.

V. COMPARATIVE ANALYSIS OF ALTERNATIVE SCHEMES

In this section, a more detailed performance comparison among the considered architectures and cancellation techniques is carried out. To this end, we apply them against a simulated clutter scenario, assuming a DVB-T illuminator of opportunity, and analyze their effectiveness in terms of clutter cancellation and moving target echoes preservation, as well as the required computational complexity, with reference to conventional approaches.

A. Performance Comparison

Assuming the same simulated scenario adopted in the previous sections, Fig. 7 shows the achievable target SCNR as a function of the input CNR level, for a target relatively close to the zero Doppler bin (-8 Hz). A disturbance with the same ICM level of Fig. 3 is assumed. All the cancellation techniques are applied after the range compression with the RF. As a reference, the performance obtained with the ECA-CS algorithm when applied according to the conventional architecture in Fig. 1(a), namely before the range compression stage with an RF, is also reported. Finally, the figure displays the maximum theoretically achievable SCNR for the considered target, which represents an upper-bound benchmark. This is accomplished assuming that the clutter is completely removed and an ideal CAF is evaluated.

As expected, both the RF+SC and RF+ECA-C schemes yield poorer SCNR results, since their cancellation capability is limited by the ICM. In addition, the target SCNR decreases as the input CNR increases, due to the stronger clutter residuals, which produce a higher interference floor.

On the other hand, the RF+ECA-CS and ECA-CS+RF offer the best SCNR results, being able to completely remove the clutter contribution up to an input CNR value of 20 dB. Beyond this level, the SCNR starts decreasing with the same slope as in the other cancellation techniques, due to the presence of clutter residues. Moreover, the two schemes show similar SCNR results, which further demonstrates that no significant performance loss occurs when applying the cancellation stage after the RF range compression stage.

The RF+ECA-CD approach yields a higher SCNR compared to the RF+ECA-C, as it provides a wider cancellation notch. However, its performance is worse than the RF+ECA-CS, despite the comparable computational cost for the selected parameter q.

Apparently, none of the evaluated schemes reaches the maximum SNR. This is due to the use of the RF at range compression stage and to the evaluation of the CAF through a batch implementation, which results in an overall SNR loss of approximately 4 dB for the considered case of a 64QAM signal [23], [25].

To further analyze the cancellation performance, Fig. 8 shows the achievable SCNR as a function of the target Doppler frequency, for a fixed input CNR $=$ 15 dB. As expected, in all cases, the SCNR increases as the target velocity increases, since the target gets far from the strongest clutter residuals located around zero Doppler.

However, due to their limited cancellation capability in the presence of ICM, the RF+ECA-C and RF+SC schemes cannot achieve SCNR values over 13 dB even for the highest Doppler frequency considered. Conversely, the RF+ECA-CS and ECA-CS+RF schemes prove to be effective and rapidly reach SCNR values over 20 dB for target Doppler frequencies beyond 10 Hz, thus significantly reducing the minimum detectable velocity of the target. The RF+ECA-CD provides intermediate performance, achieving results similar to the RF+ECA-CS case only for high Doppler frequencies.

It is worth remarking that the above results depend also on the parameters selected for the ECA-CD and ECA-CS schemes. In fact, both techniques offer the flexibility to parametrically control the width of the cancellation notch. In particular, the performance of the ECA-CD might be

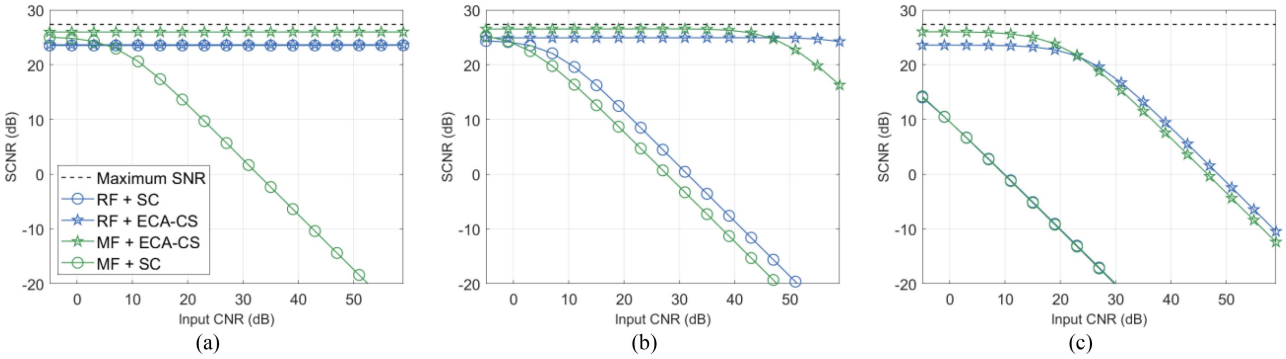

Fig. 9. Achievable SCNR for a point-like target as a function of the input CNR for a simulated clutter scenario (a) in the absence of ICM; (b) with weak ICM ($\sigma_v = 0.01$ m/s); and (c) with strong ICM ($\sigma_v = 0.1$ m/s).

further improved by increasing the number of Doppler shifted replicas q, i.e., the dimension of the clutter subspace. However, this would considerably increase the computational cost, as shown in Table I.

Moreover, it is interesting to compare the performance of the proposed alternative cancellation techniques when applied using the processing architecture in Fig. 1(b) but exploiting a MF at the range compressions stage. Fig. 9 shows the SCNR obtained for the same target considered in Fig. 7 when the SC and ECA-CS are applied after the MF (green curves) and after the RF (blue curves). In particular, Fig. 9(a) shows the results for an ideally static clutter without ICM, while Fig. 9(b) and (c) represents the case of disturbance affected, respectively, by a weak and a strong ICM, as in Fig. 4(b) and (c).

As evident from Fig. 9(a), in the presence of static clutter, the RF+SC scheme achieves a high SCNR value, independent of the input CNR, since it allows to completely remove the clutter. On the other hand, the MF+SC presents a significant performance decrease for high input CNR. In this case, in fact, the SC is unable to perfectly remove the clutter, because the echo signal at the output of the MF is no longer time-invariant, even in the absence of ICM, due to the variability of the waveform [see (10)]. This result further confirms that the simple nonadaptive SC strategy largely benefits from the proposed architecture which makes it a viable low complexity solution.

As expected, in the presence of ICM, the cancellation capability of the RF+SC scheme reduces due to the intrinsic temporal variability of the range compressed clutter signal. Fig. 9(b) shows that for a sufficiently weak ICM the RF+SC still achieves a slightly better performance compared to MF+SC. For a strong ICM instead (high variability), the RF+SC loses its advantage over the MF+SC, as visible from Fig. 9(c). This suggests that the RF+SC scheme represents a suitable and computationally effective solution, quite appropriate for scenarios with negligible ICM, at the expense of a limited loss depending on the CNR level.

In addition, Fig. 9(a) shows that, in the absence of ICM, both the MF+ECA-CS and RF+ECA-CS effectively remove the clutter, resulting in good SCNR performance for all the input CNR values. As expected, the MF+ECA-CS offers a slightly higher SCNR due to the lossless range compression based on the MF and being only affected by the loss due to the batch implementation of the CAF. In the presence of ICM, both the schemes offer better performance compared to the SC, being able to completely remove the clutter up to an input CNR value that depends on the ICM intensity, as visible by comparing Fig. 9(b) and (c). However, we recall that the RF+ECA-CS scheme requires a significantly lower computational cost compared to the MF+ECA-CS.

It is also worth noting that, for high input CNR values, the RF+ECA-CS scheme outperforms the MF+ECA-CS, as it benefits from the sidelobe reduction provided by the RF. By comparing Fig. 9(b) and (c), it is evident that this improvement depends on the ICM intensity, since the RF normalization is partially affected by the Doppler-spread disturbance. This result highlights the fact that the RF provides better performance compared to the MF in clutter limited scenarios, while suffering from a slight loss at low CNR levels, due to its mismatched range compression.

In conclusion, if a small performance degradation can be accepted in low CNR scenarios, the use of an RF in lieu of an MF enables a significant simplification of the subsequent cancellation stage. In the following subsection, we quantify this simplification by calculating the reduction in the number of floating-point operations (FLOPs) required by each cancellation technique.

B. Computational Cost Analysis

The computational complexity of each cancellation technique, when applied using both the conventional and the proposed processing architectures are reported in Fig. 10. Specifically, it is measured by evaluating the required number of FLOPs based on Table I as a function of the CIT. It is assumed that a CM requires six FLOPs, while a CA two FLOPs. As a reference, we consider a DVB-T 8K signal with $L = 8192$. In addition, for the ECA-CD, we use $q = 1$, while the ECA-CS is evaluated for $N_s = P/6$ and $N_b = 3$, which are the same parameters used for the performance evaluation in Section V-A.

As expected, all the adaptive cancellation algorithms required a reduced number of FLOPs when applied after

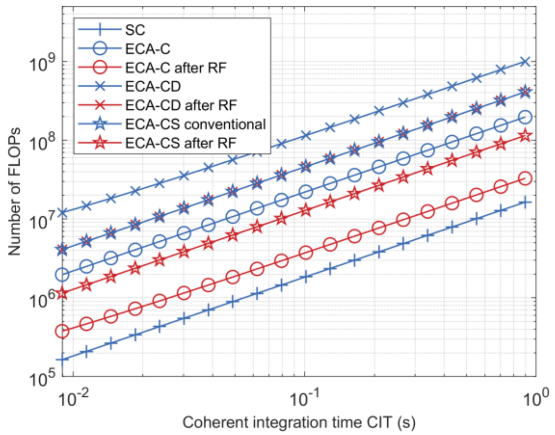

Fig. 10. Number of FLOP required by the disturbance cancellation algorithms.

the RF (compare blue curves and red curves). In particular, the improvement is constant across the evaluated CIT for the ECA-C case, which requires about six times less operations than in the conventional architecture. Similarly, the ECA-CD presents a sensible and constant decrease in the computational load of about 2.5 times for the considered parameter. On the other hand, as the results in Table I anticipated, the SC requires the lowest computational load among the considered techniques.

With the considered parameters, the computational cost of ECA-CS is between the ECA-C and the ECA-CD in its conventional application, i.e., before the range compression stage. However, it reduces approximately by a factor of 4 when applied after the RF. In fact, for the considering parameters, the number of operations required by the ECA-CS when applied after the RF is lower than the conventional ECA-C despite offering an improved performance against ICM disturbances.

It is finally worth noting that, in the considered case, with the employed parameters and using the proposed architecture, the ECA-CS requires fewer FLOPs than the ECA-CD, while providing better cancellation performance.

VI. EXPERIMENTAL RESULTS

The performance of the considered schemes is further evaluated in this section against experimental data collected by a passive receiver exploiting a DVB-T signal as illuminator of opportunity. The acquisition was performed along the shore of Civitavecchia (about 70 km North of Rome), with a PR receiver developed by the Radar and Remote Sensing Group at Sapienza University of Rome.

The experimental setup is depicted in Fig. 11. The receiver gathered an 8K DVB-T signal from a transmitter, at about 4.4 km from the receiver location, through a dedicated reference channel. In addition, a surveillance antenna, connected to a second receiving channel, was steered to the open sea with the purpose of detecting maritime targets. Table II shows the signal parameters of the experimental test.

Fig. 11. Experimental acquisition setup.

TABLE II
DVB-T Signal Parameters Description

Symbol	Description	Value
f_c	Carrier frequency	690 MHz
T_S	OFDM symbol duration	1100 μs
T_U	Useful part duration	896 μs
T_{CP}	CP duration	112 μs
C	Constellation	64QAM

TABLE III
Number of FLOPs of Each Scheme Evaluated Against Experimental Data

Scheme	Parameters	# FLOPs
RF+ECA-C	-	$5.5 * 10^7$
RF+SC	$D = 10$	$2.7 * 10^7$
ECA-CD+MF	$q = 1$	$1.7 * 10^9$
RF+ECA-CS	$N_s = P/2$ $N_b = 1$	$1.9 * 10^8$

Fig. 12 shows the range-velocity maps obtained for 1) RF+ECA-C, 2) RF+SC, 3) ECA-CD + MF, and 4) RF+ECA-CS when applied to the experimental data with a CIT of 1.5 s. Three close and slow-moving targets have been identified in the figures. In addition, the SCNR value obtained for each target is indicated and estimated as for the simulated data in Fig. 2.

As visible from Fig. 12(a) and (b), the RF+ECA-C and RF+SC scheme offer similar performance since they are both able to effectively remove the static clutter echoes. In particular, for the slowest target, the RF+ECA-C yields a higher SCNR value compared to the RF+SC. This is expected since this target is very close to zero Doppler and, as a consequence, it is affected by the nonadaptive cancellation notch of the SC, which results in a ∼2 dB SCNR degradation. Nevertheless, we observe that the RF+SC scheme yields a similar performance to the RF+ECA-C with less than half of the computational cost as shown in Table III.

On the other hand, the performance of ECA-CD+MF and RF+ECA-CS schemes is equivalent as evident from

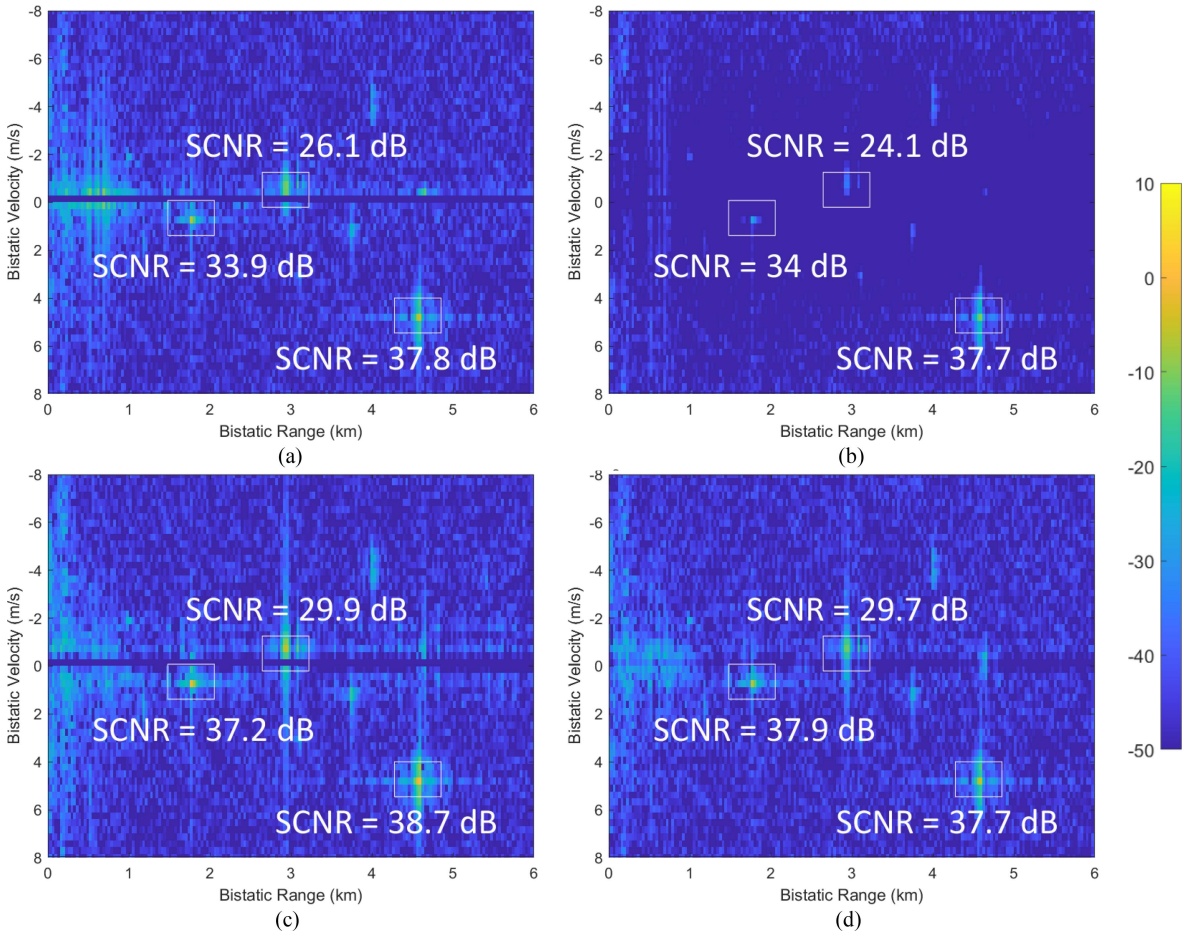

Fig. 12. Range-velocity maps obtained for a CIT of the experimental data when using (a) RF+ECA-C, (b) RF+SC, (c) ECA-CD+MF, and (d) RF+ECA-CS.

Fig. 12(c) and (d). As expected, they offer an SCNR improvement for the two slowest targets w.r.t the RF+SC and RF+ECA-C due to a wider cancellation notch and the increased robustness to ICM.

Overall, all the considered solutions yield equivalent SCNR values for the fastest target since it is not severely affected by the clutter cancellation. In particular, the ECA-CD+MF scheme offers a slight improvement of $\sim$1 dB which is due to the reduced loss measured at the range compression stage when using the MF.

While the ECA-CD+MF and RF+ECA-CS provide comparable performance, the RF+ECA-CS scheme is much faster. As evident from Table III, it yields a computational cost reduction by approximately an order of magnitude for the considered parameters and integration time. Moreover, it provides better performance compared to the RF+ECA-C despite only requiring a computational load increase by a factor of three.

VII. CONCLUSION

In this article, we investigated the impact of the RF used at the range compression stage on the OFDM-based radar signal processing chain. We showed that the computational load of adaptive disturbance cancellation techniques can be significantly reduced by exploiting the data-independent response provided by the RF since this filter equalizes the signal with respect to the structure and information content of the waveform.

Therefore, in order to leverage this characteristic, we proposed an alternative, low-complexity processing architecture for OFDM-based radar where the disturbance cancellation is applied after the range compression stage. We showed that, while the proposed approach is not equivalent to the conventional architecture, it does not suffer any performance degradation. However, using an RF for the range compression stage allows to greatly simplify the subsequent cancellation stage. This simplification was first illustrated with the ECA-C and ECA-CD, as examples of conventional adaptive cancellation techniques used with OFDM waveforms.

In addition, we proposed two alternative processing schemes that employ two different cancellation techniques with the aim to optimize either the robustness against severe clutter returns or the computational complexity: the ECA-CS for improved cancellation performance against disturbances affected by ICM, and the SC as a fast, nonadaptive algorithm. It was shown that the computational load of the ECA-CS when applied after the RF can be lower than the ECA-C used within a conventional architecture while

providing enhanced robustness against disturbance affected by ICM. In addition, it was demonstrated that the proposed architecture exploiting an RF-based range compression enables the use of a simple SC approach since it inherently guarantees a time-invariant response to static clutter.

The comparative analysis of different solutions allowed to identify the most suitable approaches in terms of both achievable performance and computational load. In particular, the RF+SC is proved to be a viable solution for clutter with negligible ICM since it offers effective clutter cancellation with an extremely limited computational load. In contrast, the RF+ECA-CS represents the best performing scheme for severe ICM clutter scenarios. These results were verified against experimental data from a PR exploiting a DVB-T illuminator of opportunity.

REFERENCES

[1] N. Levanon, "Multifrequency radar signals," in *Proc. Rec. IEEE Int. Radar Conf.*, 2000, pp. 683–688.

[2] B. Paul, A. R. Chiriyath, and D. W. Bliss, "Survey of RF communications and sensing convergence research," *IEEE Access*, vol. 5, pp. 252–270, 2017.

[3] F. Liu, C. Masouros, A. P. Petropulu, H. Griffiths, and L. Hanzo, "Joint radar and communication design: Applications, state-of-the-art, and the road ahead," *IEEE Trans. Commun.*, vol. 68, no. 6, pp. 3834–3862, Jun. 2020.

[4] L. Fan et al., "Integrated sensing and communications: Towards dual-functional wireless networks for 6G and beyond," 2021, *arXiv:2108.07165*.

[5] A. Liu et al., "A survey on fundamental limits of integrated sensing and communication," *IEEE Commun. Surv. Tut.*, vol. 24, no. 2, pp. 994–1034, Apr.–Jun. 2022.

[6] "IEE proceedings on radar sonar and navigation," *Passive Radar Syst.*, vol. 152, no. 3, pp. 106–223, Jun. 2005.

[7] R. Klemm et al., "Novel radar techniques and applications volume 1," in *Part III: Passive Multistatic Radar. SciTech*, 2017.

[8] P. Lombardo and F. Colone, "Advanced processing methods for passive bistatic radar systems," in *Principles of Modern Radar: Advanced Radar Techniques*, W. L. Melvin and J. A. Scheer, Eds. Rijeka, Croatia: SciTech, 2012, pp. 739–821.

[9] R. Saini and M. Cherniakov, "DTV signal ambiguity function analysis for radar application," *IEE Proc. Radar Sonar Navigation*, vol. 152, pp. 133–142, Jun. 2005.

[10] C. R. Berger, B. Demissie, J. Heckenbach, P. Willett, and S. Zhou, "Signal processing for passive radar using OFDM waveforms," *IEEE J. Sel. Topics Signal Process.*, vol. 4, no. 1, pp. 226–238, Feb. 2010.

[11] J. E. Palmer, H. A. Harms, S. J. Searle, and L. Davis, "DVB-T passive radar signal processing," *IEEE Trans. Signal Process.*, vol. 61, no. 8, pp. 2116–2126, Apr. 2013.

[12] F. Colone, P. Falcone, C. Bongioanni, and P. Lombardo, "WiFi-based passive bistatic radar: Data processing schemes and experimental results," *IEEE Trans. Aerosp. Electron. Syst.*, vol. 48, no. 2, pp. 1061–1079, Apr. 2012.

[13] F. Colone, D. Langellotti, and P. Lombardo, "DVB-T signal ambiguity function control for passive radars," *IEEE Trans. Aerosp. Electron. Syst.*, vol. 50, no. 1, pp. 329–347, Jan. 2014.

[14] M. A. Richards, J. A. Scheer, and W. A. Holm, *Principles of Modern Radar: Basic Principles*. Scitech Pub., Raleigh, NC, USA: SciTech, 2010, Ch. 17.

[15] F. Colone, D. W. O'Hagan, P. Lombardo, and C. J. Baker, "A multistage processing algorithm for disturbance removal and target detection in passive bistatic radar," *IEEE Trans. Aerosp. Electron. Syst.*, vol. 45, no. 2, pp. 698–722, Apr. 2009.

[16] F. Colone, C. Palmarini, T. Martelli, and E. Tilli, "Sliding extensive cancellation algorithm for disturbance removal in passive radar," *IEEE Trans. Aerosp. Electron. Syst.*, vol. 52, no. 3, pp. 1309–1326, Jun. 2016.

[17] J. L. Garry, C. J. Baker, and G. E. Smith, "Evaluation of direct signal suppression for passive radar," *IEEE Trans. Geosci. Remote Sens.*, vol. 55, no. 7, pp. 3786–3799, Jul. 2017.

[18] Z. Zhao, X. Wan, Q. Shao, Z. Gong, and F. Cheng, "Multipath clutter rejection for digital radio mondiale-based HF passive bistatic radar with OFDM waveform," *Radar, Sonar Navigation, IET*, vol. 6, no. 9, pp. 867–872, Dec. 2012.

[19] C. Schwark and D. Cristallini, "Advanced multipath clutter cancellation in OFDM-based passive radar systems," in *Proc. IEEE Radar Conf.*, 2016, pp. 1–4.

[20] C. Moscardini, D. Petri, A. Capria, M. Conti, M. Martorella, and F. Berizzi, "Batches algorithm for passive radar: A theoretical analysis," *IEEE Trans. Aerosp. Electron. Syst.*, vol. 51, no. 2, pp. 1475–1487, Apr. 2015.

[21] S. Mercier, S. Bidon, D. Roque, and C. Enderli, "Comparison of correlation-based OFDM radar receivers," *IEEE Trans. Aerosp. Electron. Syst.*, vol. 56, no. 6, pp. 4796–4813, Dec. 2020, doi: 10.1109/TAES.2020.3003704.

[22] M. Glende, "PCL-signal-processing for sidelobe reduction in case of periodical illuminator signals," in *Proc. Int. Radar Symp.*, Krakow, Poland, 2006, pp. 1–4.

[23] G. Gassier, G. Chabriel, J. Barrère, F. Briolle, and C. Jauffret, "A unifying approach for disturbance cancellation and target detection in passive radar using OFDM," *IEEE Trans. Signal Process.*, vol. 64, no. 22, pp. 5959–5971, Nov. 2016.

[24] G. Chabriel and J. Barrère, "Adaptive target detection techniques for OFDM-based passive radar exploiting spatial diversity," *IEEE Trans. Signal Process.*, vol. 65, no. 22, pp. 5873–5884, Nov. 2017.

[25] P. Wojaczek, F. Colone, D. Cristallini, and P. Lombardo, "Reciprocal-filter-based STAP for passive radar on moving platforms," *IEEE Trans. Aerosp. Electron. Syst.*, vol. 55, no. 2, pp. 967–988, Apr. 2019.

[26] G. P. Blasone, F. Colone, P. Lombardo, P. Wojaczek, and D. Cristallini, "Passive radar DPCA schemes with adaptive channel calibration," *IEEE Trans. Aerosp. Electron. Syst.*, vol. 56, no. 5, pp. 4014–4034, Oct. 2020.

[27] M. A. Richards, *Fundamentals of Radar Signal Processing*, 2nd ed. New York, NY, USA: McGraw-Hill, 2014, Ch. 5.

[28] J. Trujillo Rodriguez, G. P. Blasone, F. Colone, and P. Lombardo, "A simple clutter suppression approach for OFDM-based passive radar exploiting reciprocal filter," in *Proc. Radar: Int. Conf. Radar Syst.*, 2022.

[29] C. Sturm, T. Zwick, and W. Wiesbeck, "An OFDM system concept for joint radar and communications operations," in *Proc. IEEE 69th Veh. Technol. Conf.*, 2009, pp. 1–5.

[30] F. Colone, F. Filippini, M. Di Seglio, and K. Chetty, "On the use of reciprocal filter against wifi packets for passive radar," *IEEE Trans. Aerosp. Electron. Syst.*, vol. 58, no. 4, pp. 2746–2761, Aug. 2022.

[31] J. Trujillo Rodriguez, F. Colone, and P. Lombardo, "Supervised reciprocal filter for OFDM radar signal processing," *IEEE Trans. Aerosp. Electron. Syst.*, early access, Jan. 19, 2023, doi: 10.1109/TAES.2023.3235317.

[32] J. Trujillo Rodriguez, F. Colone, and P. Lombardo, "Loaded reciprocal filter for OFDM-based passive radar signal processing," in *Proc. IEEE Radar Conf.*, 2022, pp. 1–6.

Javier Trujillo Rodriguez (Student Member, IEEE) received the B.Sc. degree in telecommunications engineering from the Instituto Balseiro, San Carlos de Bariloche, Argentina, in 2018. He is currently working toward the Ph.D. degree in radar and remote sensing with the DIET Department, Sapienza University of Rome, Rome, Italy.

In 2019, he worked as a Data Scientist with the Telefonica Argentina. His research interests include adaptive signal processing for OFDM-based and passive bistatic radar systems. He has been involved in research projects funded by the Italian Government.

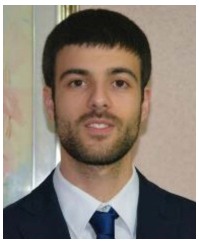

Giovanni Paolo Blasone (Member, IEEE) received the M.Sc. degree (Hons.) in telecommunication engineering and the Ph.D. degree (Hons.) in radar and remote sensing from the Sapienza University of Rome, Rome, Italy, in 2016 and 2021, respectively.

Since 2021, he has been a Postdoctoral Researcher with the Department of Information Engineering, Electronics and Telecommunications, Sapienza University of Rome. His research interests include adaptive signal processing for multichannel radar systems and passive radar GMTI. He has been involved in research projects funded by the Italian Space Agency, the Italian Ministry of Research, and the National Radar Industry.

Dr. Blasone was a finalist in the Student Paper Competition at the 2020 IEEE International Radar Conference, in the 3MT Contest at the 2020 IEEE Radar Conference, and in the 2021 GTTI Ph.D. Award.

Fabiola Colone (Senior Member, IEEE) received the laurea degree (B.S.+M.S.) in telecommunications engineering and the Ph.D. degree in remote sensing from the Sapienza University of Rome, Rome, Italy, in 2002 and 2006, respectively.

She joined the DIET Department, Sapienza University of Rome as a Research Associate in 2006. From 2006 to 2007, she was a Visiting Scientist with the Electronic and Electrical Engineering Department, University College London, London, U.K. She is currently a Full Professor with the Faculty of Information Engineering, Informatics, and Statistics, Sapienza University of Rome. Her research interests include radar systems and signal processing. She has been involved, with scientific responsibility roles, in research projects funded by the European Commission, the European Defence Agency, the Italian Space Agency, the Italian Ministry of Research, and many radar/ICT companies. Her research has been reported in more than 160 publications in international technical journals, book chapters, and conference proceedings.

Dr. Colone is coeditor of the book "Radar Countermeasures for Unmanned Aerial Vehicles," IET Publisher. She has been corecipient of the 2018 Premium Award for Best Paper in IET Radar, Sonar & Navigation.

Since 2017, she has been a member of the Board of Governors of IEEE Aerospace and Electronic System Society in which she has served as a Vice-President for Member Services, and Editor-in-Chief for IEEE AESS QEB Newsletters. She has been a member of IEEE AESS Radar System Panel since 2019. She is an Associate Editor in Chief for IEEE TRANSACTIONS ON RADAR SYSTEMS. She was an Associate Editor for IEEE TRANSACTIONS ON SIGNAL PROCESSING and is a member of the Editorial Board of the *International Journal of Electronics and Communications* (Elsevier). She has served in the organizing committee and in the technical program committee of many international conferences. She was a Technical Co-Chair of IEEE 2021 Radar Conference (Atlanta, GA, USA) and of the European Radar Conference EuRAD 2022 (Milan, Italy).

Pierfrancesco Lombardo (Senior Member, IEEE) received the graduate degree in electronic engineering and the Ph.D. degree in remote sensing from the University of Rome "La Sapienza," Rome, Italy, in 1991 and 1995, respectively.

After serving with the Official Test Centre of the Italian Air Force in 1992, he was an Associate with the Birmingham University, Birmingham, U.K., and with the Defence Research Agency, Malvern, U.K., in 1994. In 1995, he was a Research Associate with the Syracuse University, Syracuse, NY, USA. In 1996, he joined the University of Rome "La Sapienza," where he is currently a Full Professor. He is involved in, and coordinates, research projects funded by European and National Research Agencies and national industries. He leads the "Radar, Remote Sensing, and Navigation" group, University of Rome "La Sapienza." He chairs the Cosmo-SkyMed consulting group for the Italian Space Agency. His research interests include radar adaptive signal processing, radar clutter modeling, radar coherent detection, passive radar and multistatic radar, SAR processing, and radio-localization systems. His research has been reported in more than 280 publications in international technical journals and conferences and 5 book chapters.

Dr. Lombardo was a corecipient of the Barry Carlton Award (Best Paper) of IEEE TRANSACTIONS ON AEROSPACE AND ELECTRONIC SYSTEMS in 2001 and of the Best Paper Award for IEEE TRANSACTION ON GEOSCIENCE AND REMOTE SENSING in 2003. He served the technical committee of many international conferences on radar systems and signal processing. He was a Technical Committee Chairman of IEEE/ISPRS Workshop on Remote Sensing and Data Fusion over Urban Areas URBAN'2001, Rome, URBAN'2003, Berlin, and URBAN'2005, Tempe, USA, and also a Technical Chairman of IEEE Radar Conference 2008. He has been an Associate Editor for Radar Systems for IEEE TRANSACTIONS ON AEROSPACE AND ELECTRONIC SYSTEMS since 2001, and a Technical Editor for Radar System since 2016. He is a member of IEEE AES Radar System Panel and the Editorial Board of IET Proceedings on Radar, Sonar, and Navigation.

Open Access provided by 'Università degli Studi di Roma "La Sapienza" 2' within the CRUI CARE Agreement